frontiers in Chemistry

ORIGINAL RESEARCH
published: 01 December 2020
doi: 10.3389/fchem.2020.598095

Quinazolinones as Competitive Inhibitors of Carbonic Anhydrase-II (Human and Bovine): Synthesis, *in-vitro*, *in-silico*, Selectivity, and Kinetics Studies

Ajmal Khan[1], Majid Khan[1,2], Sobia Ahsan Halim[1], Zulfiqar Ali Khan[3], Zahid Shafiq[4] and Ahmed Al-Harrasi[1]**

[1] Natural and Medical Sciences Research Center, University of Nizwa, Nizwa, Oman, [2] International Center for Chemical and Biological Sciences, H. E. J. Research Institute of Chemistry, University of Karachi, Karachi, Pakistan, [3] Department of Chemistry, Government College University, Faisalabad, Pakistan, [4] Institute of Chemical Sciences, Bahauddin Zakariya University, Multan, Pakistan

OPEN ACCESS

Edited by:
Imtiaz Khan,
The University of Manchester,
United Kingdom

Reviewed by:
Mohammed El-Gamal,
University of Sharjah,
United Arab Emirates
Dr. Suresh Reddy Chidipudi,
Spiro Organics Private Limited, India

***Correspondence:**
Zahid Shafiq
zahidshafiq@bzu.edu.pk
Ahmed Al-Harrasi
aharrasi@unizwa.edu.om

Specialty section:
This article was submitted to Medicinal and Pharmaceutical Chemistry, a section of the journal Frontiers in Chemistry

Received: 23 August 2020
Accepted: 28 October 2020
Published: 01 December 2020

Citation:
Khan A, Khan M, Halim SA, Khan ZA, Shafiq Z and Al-Harrasi A (2020) Quinazolinones as Competitive Inhibitors of Carbonic Anhydrase-II (Human and Bovine): Synthesis, in-vitro, in-silico, Selectivity, and Kinetics Studies. Front. Chem. 8:598095. doi: 10.3389/fchem.2020.598095

Carbonic anhydrase-II (CA-II) is associated with glaucoma, malignant brain tumors, and renal, gastric, and pancreatic carcinomas and is mainly involved in the regulation of the bicarbonate concentration in the eyes. CA-II inhibitors can be used to reduce the intraocular pressure usually associated with glaucoma. In search of potent CA-II inhibitors, a series of quinazolinones derivatives (**4a-p**) were synthesized and characterized by IR and NMR spectroscopy. The inhibitory potential of all the compounds was evaluated against bovine carbonic anhydrase-II (*b*CA-II) and human carbonic anhydrase-II (*h*CA-II), and compounds displayed moderate to significant inhibition with IC_{50} values of 8.9–67.3 and 14.0–59.6 μM, respectively. A preliminary structure-activity relationship suggested that the presence of a nitro group on the phenyl ring at R position contributes significantly to the overall activity. Kinetics studies of the most active inhibitor, **4d**, against both *b*CA-II and *h*CA-II were performed to investigate the mode of inhibition and to determine the inhibition constants (Ki). According to the kinetics results, **4d** is a competitive inhibitor of *b*CA-II and *h*CA-II with Ki values of 13.0 ± 0.013 and 14.25 ± 0.017 μM, respectively. However, the selectivity index reflects that the compounds **4g** and **4o** are more selective for *h*CA-II. The binding mode of these compounds within the active sites of *b*CA-II and *h*CA-II was investigated by structure-based molecular docking. The docking results are in complete agreement with the experimental findings.

Keywords: quinazolinones, bovine carbonic anhydrase-II, human carbonic anhydrase-II, structure-activity relationship, kinetics, molecular docking

INTRODUCTION

Carbonic anhydrases (CAs, EC 4.2.1.1) are zinc-containing metallo-enzymes, found in animals, plants, algae, archaea, and eubacteria. CAs are encoded by three gene families, α-CA, β-CA, and γ-CA, that are evolutionarily unrelated (Hewett-Emmett, 2000; Jakubowski et al., 2018). These metallo-enzymes use zinc as a cofactor for the reversible inter-conversion of carbon dioxide and bicarbonate, while α-CAs possess high versatility, being able to catalyze other hydrolytic

processes (Hewett-Emmett, 2000). Carbonic anhydrases are a class of hydrolase enzymes (Pocker and Meany, 1967; Arslan, 2001). In humans, more than 16 isoforms of carbonic anhydrase (*h*CA) are present (Shank et al., 2005; Shaik et al., 2019). CAs are involved in different physiological and pathological processes (Lindskog, 1997; Aggarwal et al., 2013; Ozensoy Guler et al., 2016). Consequently, these enzymes are interesting therapeutic targets for the treatment of pathological disorders (Chegwidden et al., 2000; Krishnamurthy et al., 2008; Supuran, 2008). CA-II is mainly involved in the regulation of the bicarbonate concentration in the eyes. CA-II inhibitors can be used to reduce the intraocular pressure usually associated with glaucoma (Supuran and Scozzafava, 2007; Pastorekova and Supuran, 2014; Ruusuvuori and Kaila, 2014; Zaraei et al., 2019). Moreover, CA-II is also expressed in malignant brain tumors (Parkkila et al., 1995) and renal, gastritis, and pancreatic carcinomas (Frazier et al., 1990; Pastorekova et al., 1997; Parkkila et al., 2000). The inhibitors of CA-II have also been considered as an adjunct in cancer chemotherapy (Zaraei et al., 2019).

These highly abundant proteins are involved in crucial physiological processes related with respiration. These enzymes are mainly involved in pH/CO_2 homeostasis, secretion of electrolytes in tissues/organs, and transportation of CO_2 and bicarbonate between the lungs and metabolizing tissues. Other than that these enzymes are also involved in many other physiological or pathological processes, such as bone resorption, gluconeogenesis, calcification, lipogenesis and ureagenesis, and tumorgenicity (Hewett-Emmett, 2000). CA-II has also been involved in glaucoma, epilepsy, leukemia, and cystic fibrosis (Achal and Pan, 2011; Sentürk et al., 2011).

Quinazolinones are *N*-containing heterocyclic compounds that are widely distributed in nature, including in plants and microorganisms (He et al., 2017). Quinazolinone emerged as a privileged class of heterocyclic compounds with an increasing number of drug candidates and is regularly used in medicinal chemistry (Khan et al., 2014, 2015, 2016). The 2,3-Disubstituted quinazolinones retain anticancer (Al-Suwaidan et al., 2013), anticonvulsant (Gawad et al., 2011), anti-microbial (Al-Amiery et al., 2014), and anti-inflammatory activities (Alaa et al., 2016). Several derivatives of 3-(4-Aminosulfonyl)-phenyl-2-mercapto-substituted-4(3*H*)-quinazolinones (**A**) are reported for *h*CA-I (KIs = 135–282 nM), *h*CA-II (KIs = 0.25–10.8 nM), *h*CA-IX (KIs of 3.7–50.4 nM), and CA-XII (KIs of 0.60–52.9 nM) as potent inhibitors (Alafeefy et al., 2016). Several other 2-[(3-substituted-4(3*H*)-quinazolinon-2-yl)thio]-*N*-(4-sulfamoylphenyl)acetamides (**B**) derivatives also showed potent inhibition of α-CA, from *Vibrio cholerae* (VchCA) and human "*h*CA-I" and "*h*CA-II," at a nanomolar level (Alafeefy et al., 2014) (**Figure 1**). Recently, 2-[(3-Benzyl-6,7-dimethoxy-4-(3*H*)-quinazolinon-2-yl)thio]-*N*-(4-sulfamoylphenyl)propanamide was also reported for *h*CA-II (KI, 3.30 nM) inhibition (El-Azab et al., 2019).

In this study, we report the synthesis and *in-vitro* bovine carbonic anhydrase-II (*b*CA-II) and human carbonic anhydrase-II (*h*CA-II) inhibitory activities of a series of quinazolinone analogs. Furthermore, the mode of inhibition was further explored by kinetic studies of the active analogs. Additionally, molecular docking studies were carried out to predict the main structural features responsible for the anti-CA-II activities of the compounds to predict the structure-activity relationships.

EXPERIMENTAL

Chemistry

The chemicals used in this study were purchased from Sigma and Aldrich in extra purified form. Melting points for all compounds were recorded by Büchi 434 melting point apparatus. FT-IR spectra (KBr disks) were measured on a Bruker FT-IR IFS48 spectrophotometer. NMR spectra were recorded on Bruker Avance 400 spectrometers in DMSO-d^6. The chromatograms were visualized under UV light irradiation. The CHN analysis was performed on a Carlo Erba Strumentazione-Mod-1106.

General Procedure for Synthesis of 2-substituted-4*H*-benzo[*d*][1,3]oxazin-4-ones (3a-p) (Bari et al., 2020)

To an 100 mL round bottom flask, anthranilic acid **1** (0.01 mol) and dry pyridine (30 mL) were added at room temperature with stirring. The solution was cooled to 0°C, followed by dropwise addition of the corresponding aromatic acid chloride **2a-p** (0.02 mol) in 10 mL of dry pyridine with constant stirring. After this addition, the reaction mixture was stirred for a further half an hour at room temperature and set aside for 1 h. The product, obtained as a pasty mass, was diluted with ice cold water (50 mL) and treated with aqueous sodium bicarbonate solution.

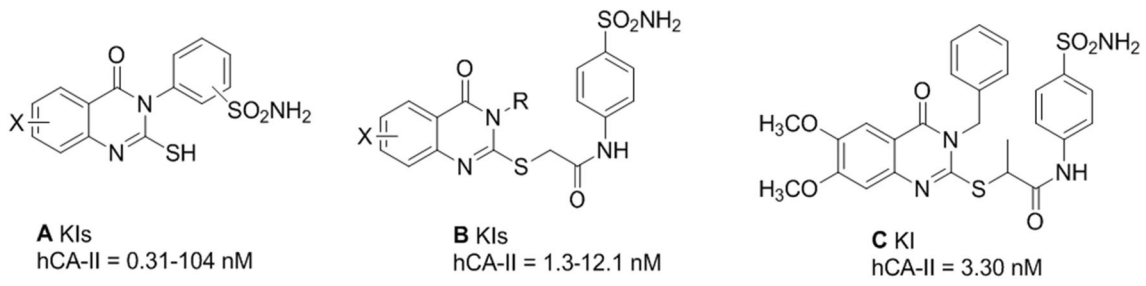

FIGURE 1 | Reported inhibitors of CA-II **(A–C)**.

When the effervescence ceased, the precipitate obtained was filtered and washed with water. The crude benzoxazine obtained was dried and recrystallized from aqueous ethanol.

General Procedure for the Synthesis of Quinazolinone (4a-p) (Panicker et al., 2010)

To a 50 mL round bottom flask fitted with reflux condenser were added 2-substituted-4*H*-benzo[*d*][1,3]oxazin-4-one (0.01 mol) and hydrazine hydrate (0.06 mol) in excess. The reaction mixture was heated under reflux in an oil bath for 10–16 h. The course of the reaction was monitored by thin layer chromatography (TLC). After completion of the reaction as checked by TLC, the reaction mixture was cooled and separated solids were collected by filtration, washed with water/hexane, dried, and purified by column chromatography (methanol/chloroform/water, 10:2:1) to afford the corresponding quinazolinones **4a-p**.

Experimental Data

3-Amino-2-Phenylquinazolin-4(3*H*)-one (4a) (Panicker et al., 2010)

Yield: 82%; mp: 200–202°C; FT-IR (υ_{max}, KBR, cm^{-1}): 3,319, 3,051, 1,660, 1,603, 1,490, 1258; ^{1}H NMR (400 MHz, DMSO-d^6, δ, ppm): 5.36 (s, 2H), 7.47–8.18 (m, 9H); Anal. Calcd. for $C_{14}H_{11}N_3O$: C, 70.88; H, 4.64; N, 17.72. Found: C, 70.92; H, 4.67; N, 17.68.

3-Amino-2-(Napthalen-1-yl) Quinazolin-4(3*H*)-one (4b)

Yield: 80%; m.p: 215–216°C; FT-IR (υ_{max}, KBR, cm^{-1}): 3,316, 3,053, 1,662, 1,600, 1,493, 1,257; ^{1}H NMR (400 MHz, DMSO-d^6, δ, ppm): 5.42 (2H, s) 7.55–7.64 (4H, m), 7.7–7.88 (4H, m), 8.20 (1H, d, $J = 7.4$ Hz),), 8.42 (1H, d, $J = 7.2$ Hz), 8.38 (1H, d, $J = 7.2$ Hz); Anal. Calcd. for $C_{14}H_{11}N_3O$: C, 70.88; H, 4.64; N, 17.72. Found: C, 70.92; H, 4.67; N, 17.68.

3-Amino-2-(2-Nitrophenyl) Quinazolin-4(3*H*)-one (4c) (Pandit and Dodiya, 2013)

Yield: 77%; m.p: 180–182°C; FT-IR (υ_{max}, KBR, cm^{-1}): 3,309, 3,053, 1,673, 1,603, 1,548, 1,489, 1,354, 1,250; 701; ^{1}H NMR (400 MHz, DMSO-d^6, δ, ppm): 5.43 (2H, s), 7.51–7.63 (4H, m), 7.91–8.02 (4H, m); Anal. Calcd. for $C_{14}H_{10}N_4O_3$: C, 59.57; H, 3.57; N, 19.85; Found: C, 59.56; H, 3.58; N, 19.85.

3-Amino-2-(3-Nitrophenyl) Quinazolin-4(3*H*)-one (4d) (Pandit and Dodiya, 2013)

Yield: 84%; m.p: 206–208°C; FT-IR (υ_{max}, KBR, cm^{-1}): 3,308, 3,053, 1,675, 1,600; 1,548, 1,490, 1,248, 1,355, 703; ^{1}H NMR (400 MHz, DMSO-d^6, δ, ppm): 5.48 (s, 2H), 7.62–7.68 (3H, m), 8.07 (1H, d, $J = 7.4$ Hz), 8.2 (1H, d, $J = 7.2$ Hz), 8.27 (1H, d, $J = 7.8$ Hz), 8.56 (1H, s); Anal. Calcd. for $C_{14}H_{10}N_4O_3$: C, 59.57; H, 3.57; N, 19.85. Found: C, 59.56; H, 3.58; N, 19.85.

3-Amino-2-(4-nitrophenyl) quinazolin-4(3*H*)-one (4e) (Pandit and Dodiya, 2013)

Yield: 76%; m.p: 224–225°C; FT-IR (υ_{max}, KBR, cm^{-1}): 3,307, 3,053, 1,670, 1,603, 1,548, 1,488, 1,353, 1,250; 708; ^{1}H NMR (400 MHz, DMSO-d^6, δ, ppm): 5.42 (2H, s), 7.66–7.71 (3H, m), 8.06 (1H, d, J= 7.2 Hz), 8.12 (2H, d, $J = 7.8$ Hz), 8.26 (2H, d, $J = 7.8$ Hz); Anal. Calcd. for $C_{14}H_{10}N_4O_3$: C, 59.57; H, 3.57; N, 19.85. Found: C, 59.56; H, 3.58; N, 19.85.

3-Amino-2-(2-Bromophenyl) Quinazolin-4(3*H*)-one (4f)

Yield: 79%; m.p: 204–206°C; FT-IR (υ_{max}, KBR, cm^{-1}): 3,300, 3,053, 1,673, 1,610, 1,010, 690; ^{1}H NMR (400 MHz, DMSO-d^6, δ, ppm): 5.25 (2H, s), 7.35–7.39 (2H, t, $J = 7.2$ Hz), 8.06 (1H, d, $J = 8.1$ Hz), 7.58–7.66 (5H, m); *Anal.* Calcd for $C_{14}H_{10}BrN_3O$: C, 53.19; H, 3.19; N, 13.29. Found: C, 53.17; H, 3.20; N, 13.28.

3-Amino-2-(4-Bromophenyl) Quinazolin-4(3*H*)-one (4g)

Yield: 81%; m.p: 184–185°C; FT-IR (υ_{max}, KBR, cm^{-1}): 3,300, 3,053, 1,676, 1,610, 1,010, 690; ^{1}H NMR (400 MHz, DMSO-d^6, δ, ppm): 5.26 (2H, s), 7.52 (2H, d, $J = 7.45$ Hz), 7.61–7.67 (3H, m), 7.74 (2H, d, $J = 7.6$ Hz), 8.1 (1H, d, $J = 7.55$ Hz); *Anal.* Calcd for $C_{14}H_{10}BrN_3O$: C, 53.19; H, 3.19; N, 13.29. Found: C, 53.17; H, 3.20; N, 13.28.

3-Amino-2-(4-Methylphenyl) Quinazolin-4(3*H*)-one (4h) (Babu et al., 2014)

Yield: 85%; mp: 294–296°C; FT-IR (υ_{max}, KBR, cm^{-1}): 3,300, 3,053, 2,948, 1,676, 1,610, 1,496; ^{1}H NMR (400 MHz, DMSO-d^6, δ, ppm): 2.34 (3H, s), 4.93 (2H, s), 8.08 (1H, d, $J = 7.2$ Hz), 7.28 (2H,d, $J = 7.8$ Hz), 7.44 (2H, d, $J = 7.8$ Hz), 7.55-7.67 (3H, m); *Anal.* Calcd for $C_{15}H_{13}N_3O$: C, 71.70; H, 5.21; N, 16.72. Found: C, 71.71; H, 5.20; N, 16.73.

3-Amino-2-(2-Fluorophenyl) Quinazolin-4(3*H*)-one (4i)

Yield: 84%; m.p: 169–170°C; (υ_{max}, KBR, cm^{-1}): 3,308, 3,053, 1,681, 1,610; 1,329, 506 ^{1}H NMR (400 MHz, DMSO-d^6, δ, ppm): 4.98 (2H, s), 8.20 (1H, d, $J = 7.2$ Hz), 7.77 (1H, bd, $J = 8.4$ Hz), 7.59–7.67 (4H, m), 7.29–7.36 (2H, m); *Anal.* Calcd for $C_{14}H_{10}FN_3O$: C, 65.88; H, 3.95; N, 16.46. Found: C, 65.89; H, 3.94; N, 16.47

3-Amino-2-(3-Fluorophenyl) Quinazolin-4(3*H*)-one (4j)

Yield: 78%; m.p: 164–165°C; FT-IR (υ_{max}, KBR, cm^{-1}): 3,310, 3,053, 1,679, 1,610; 1,335, 502; ^{1}H NMR (400 MHz, DMSO-d6, δ, ppm): 5.52 (2H, s), 8.01 (1H, d, $J = 7.2$Hz), 7.78 (1H, d, $J = 7.8$ Hz), 7.58–7.66 (4H, m), 7.32 (1H, t, $J = 7.8$ Hz); *Anal.* Calcd for $C_{14}H_{10}FN_3O$: C, 65.88; H, 3.95; N, 16.46. Found: C, 65.89; H, 3.94; N, 16.47.

3-Amino-2-(4-Fluorophenyl) Quinazolin-4(3*H*)-one (4k)

Yield: 81%; m.p: 176–178°C; FT-IR (υ_{max}, KBR, cm^{-1}): 3,310, 3,053, 1,680, 1,610; 1,335, 502; ^{1}H NMR (400 MHz, DMSO-d^6, δ, ppm): 5.38 (s, 2H), 7.26–7.30 (2H, m), 7.41–7.46 (2H, m), 7.53–7.56 (2H, m), 8.26 (1H,d, $J = 7.5$ Hz); *Anal.* Calcd for $C_{14}H_{10}FN_3O$: C, 65.88; H, 3.95; N, 16.46. Found: C, 65.87; H, 3.94; N, 16.47.

3-Amino-2-(2-Chlorophenyl) Quinazolin-4(3*H*)-one (4l) (Pandit and Dodiya, 2013)

Yield: 85%; m.p: 160–162°C; FT-IR (υ_{max}, KBR, cm^{-1}): 3,310, 3,053, 1,689, 1,610; ^{1}H NMR (400 MHz, DMSO-d^6, δ, ppm): 5.08 (2H, s), 7.41–7.45 (2H, t, $J = 7.3$ Hz), 7.48 (1H, d, $J = 7.3$ Hz) 7.54 (1H, d, $J = 7.3$ Hz), 7.58–7.69 (3H, m), 8.07 (1H, d, $J = 7.2$ Hz);

Anal. Calcd for $C_{14}H_{10}ClN_3O$: C, 61.89; H, 3.71; N, 15.47. Found C, 61.87; H, 3.73; N, 15.47.

3-Amino-2-(3-Chlorophenyl) Quinazolin-4(3*H*)-one (4m) (Pandit and Dodiya, 2013)

Yield: 79%; m.p: 144–145°C; FT-IR (υ_{max}, KBR, cm^{-1}): 3,307, 3,210, 3,051, 2,993, 1,668, 1,591, 1,252, 1,123; 458; ^1H NMR (400 MHz, DMSO-d^6, δ, ppm): 5.33 (2H, s), 8.14 (1H, d, $J = 7.2$ Hz), 7.84 (1H, s), 7.63–7.68 (3H, m), 7.46–7.52 (3H, m); *Anal.* Calcd for $C_{14}H_{10}ClN_3O$: C, 61.89; H, 3.71; N, 15.47. Found C, 61.87; H, 3.73; N, 15.47.

3-Amino-2-(4-Chlorophenyl) Quinazolin-4(3*H*)-one (4n) (Castillo et al., 2012)

Yield: 86%; m.p: 165–166°C; FT-IR (υ_{max}, KBR, cm^{-1}): 3,310, 3,213, 3,053, 2,990, 1,670, 1,591, 1,252, 1,123; 462 ^1H NMR (400 MHz, DMSO-d^6, δ, ppm): 4.86 (s, 2H) 7.34 (2H, d, $J = 7.4$ Hz), 7.56 (2H, d, $J = 7.4$ Hz), 7.68–7.75 (3H, m), 8.04 (1H, d, $J = 7.2$ Hz); Anal. Calcd for $C_{14}H_{10}ClN_3O$: C, 61.89; H, 3.71; N, 15.47. Found C, 61.87; H, 3.73; N, 15.47.

3-Amino-2-(4-Methoxyphenyl) Quinazolin-4(3*H*)-one (4o) (Pandit and Dodiya, 2013)

Yield: 88%; m.p: 221–223°C; FT-IR (υ_{max}, KBR, cm^{-1}): 3,310, 3,053, 2,940, 1,689, 1,610, 1,490; ^1H NMR (400 MHz, DMSO-d^6, δ, ppm): 4.92 (2H,s), 3.76 (3H, s), 6.96 (2H, d, J =7.5 Hz), 7.34 (2H, d, $J = 7.5$ Hz),7.60–7.68 (3H, m), 8.09 (1H, d, $J = 7.3$ Hz); Anal. Calcd. for $C_{15}H_{13}N_3O_2$: C, 67.40; H, 4.90; N, 15.72; Found C, 67.42; H, 4.88; N, 15.71.

3-Amino-2-(3,4,5-Trimethoxyphenyl) Quinazolin-4(3*H*)-one (4p)

Yield: 78%; m.p: 221–222°C; FT-IR (υ_{max}, KBR, cm^{-1}): 3,310, 3,053, 2,950, 1,689, 1,610, 1,495; ^1H NMR (400 MHz, DMSO-d^6, δ, ppm): 3.79 (6H, s), 3.82 (3H, s), 4.88 (2H, s), 6.62 (2H, s), 7.48–7.52 (3H, m), 8.01 (1H, d, $J = 7.3$ Hz); Anal. Calcd. for $C_{17}H_{17}N_3O_4$: C, 62.38; H, 5.23; N, 12.84; Found C, 62.38; H, 5.24; N, 12.83.

In-vitro Assay Protocol

*In-vitro b*CA-II and *h*CA-II activities were measured by following the spectrophotometric method described by Pocker and Meany with slight modifications (Pocker and Meany, 1967; Ur Rehman et al., 2020). The spectrophotometric assay was conducted in HEPES-Tris buffer of pH 7.4 (20 mM) at 25°C. Each inhibitory well-consisted of 140 μL of HEPES-Tris buffer solution, 20 μL of *b*CA-II enzyme solution (0.1 mg/mL HEPES-Tris buffer), and 20 μL of test compound in HPLC grade DMSO (maintain 10% of the final concentration). The mixture solution was pre-incubated for 15 min at 25°C. Substrate *p*-nitrophenyl acetate (*p*-NPA) (0.7 mM) was prepared in HPLC grade methanol and the reaction was started by adding 20 μL to a well in a 96-well-plate. The amount of product formed was measured for 30 min continuously at 1 min intervals at 400 nm in a 96-well-plate using xMARK microplate spectrophotometer, Bio-Rad (USA). The activity of the controlled compound was taken as 100%. All experiments were carried out in triplicates of each used concentration, and results are represented as a mean of the triplicate.

Molecular Docking Protocol

The docking studies were performed on the crystal structures of *b*CA-II (1V9E, resolution = 1.95 Å) (Saito et al., 2004) and *h*CA-II (1BN1, resolution = 2.1 Å) (Boriack-Sjodin et al., 1998). The selected target receptors were retrieved from Protein Data Bank (www.rcsb.org) in PDB format. Chain A of each protein (1V9E and 1BN1) was chosen for docking. For the molecular docking simulation, Molecular Operating Environment (MOE) docking suite was used (MOEv2014.09). The crystal structures were prepared using Protein Preparation Wizard implemented in the MOE with the default settings. Hydrogen atoms were added in the MOE using protonate 3D protocol and the protein structures were minimized with an MMFF94x force field until an RMSD gradient of 0.1 $kcal{\cdot}mol^{-1}Å^{-1}$ was achieved. The 3D-structures of ligands were prepared by Chemdraw and minimized by default option of MOE (Force field = MMFF94x, RMS gradient = 0.1 $kcal{\cdot}mol^{-1}Å^{-1}$). For docking, Triangle Matcher placement method and London dG scoring function were applied (Edelsbrunner, 1992; Naïm et al., 2007). After docking, thirty docked poses of each compound were saved and the best-scoring docked pose of each ligand was visualized.

RESULTS AND DISCUSSION

Chemistry

The target compounds were synthesized according to the route depicted in **Scheme 1**. Anthranilic acid **1** was treated with corresponding acid chlorides (**2a-p**) in the presence of pyridine to form precursor heterocycle (**3a-p**) via literature method (**Scheme 1**) (Bari et al., 2020). The corresponding benzoxazinones were refluxed in excess of hydrazine hydrate to furnish the 3-Amino-2-aryl quinazolin-4(3*H*)-ones (**4a-p**) in

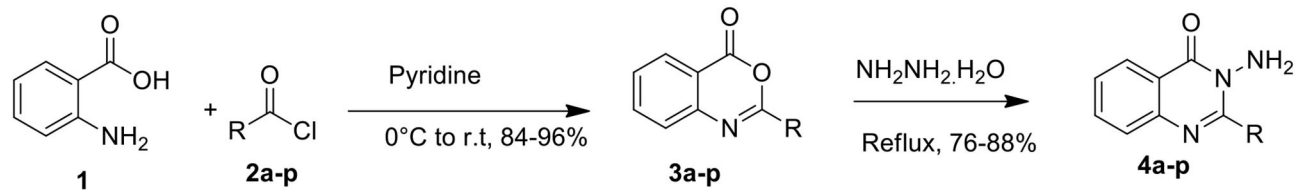

SCHEME 1 | Synthesis of quinazolinone derivatives.

moderate to excellent yields of 76–88% (**Table 1**) (Panicker et al., 2010).

The structures of compounds (**4a-p**) were established using microanalysis (CHN) and spectral data, i.e., IR and ^{1}H NMR. The C=N band in FTIR appeared in the range of 1,489–1,521 cm^{-1}. Moreover, the carbonyl group of compounds (**4a-p**) appeared at 1,660–1,689 cm^{-1}. The amino moiety (-NH_2) of compounds (**4a-p**) was verified by the characteristic peak at 3,300–3,319 cm^{-1} in FT-IR spectra. The amino-moiety of compounds (**4a-p**) was verified by ^{1}H NMR spectra which appeared as a singlet for amino protons in a range from δ 4.92–5.52 *ppm*. The spectral data of other aromatic and aliphatic protons was also in accordance with the structures of anticipated compounds. CHN analysis also supported the anticipated structures (**4a-p**) and the observed values were in good agreement with the values found.

TABLE 1 | Different analogs, % yield, and reaction time of quinazolinones.

Entry	Compounds	R	% Yields	Reaction time(h)
1	**4a**	Phenyl	82	12
2	**4b**	1*r*- Naphthyl	80	10
3	**4c**	2*r*-Nitrophenyl	77	16
4	**4d**	3*r*-Nitrophenyl	84	20
5	**4e**	4*r*-Nitrophenyl	76	20
6	**4f**	2*r*-Bromophenyl	79	11
7	**4g**	4*r*-Bromophenyl	81	12
8	**4h**	4*r*-Methylphenyl	85	8
9	**4i**	2*r*-Fluorophenyl	84	12
10	**4j**	3*r*-Fluorphenyl	78	14
11	**4k**	4*r*-Fluorophenyl	81	10
12	**4l**	2*r*-Chlorophenyl	85	10
13	**4m**	3*r*-Chlorophenyl	79	12
14	**4n**	4*r*-Chlorophenyl	86	10
15	**4o**	4*r*-Methoxyphenyl	88	15
16	**4p**	3*r*,4*r*,5*r*-Trimethoxyphenyl	78	13

Biology

*In-vitro b*CA-II and *h*CA-II inhibitions

All quinazolinone analogs (**4a-p**) were evaluated against bovine carbonic anhydrase-II (*b*CA-II) and human carbonic anhydrase-II (*h*CA-II) for their ability to act as an inhibitor of CA-II. All the assays were carried out at a micromolar level using acetazolamide as a standard inhibitor. After initial screening, all the analogs demonstrated significant inhibitory activity against *b*CA-II with IC_{50} values in the range of 8.9 ± 0.31 −67.3 ± 0.42 μM, except compounds **4i** and **4o**, which were found to be inactive (**Table 2**). Moreover, compounds **4c**, **4e**, **4f**, **4l**, and **4m** showed more superior activity than the standard drug 'acetazolamide' (IC_{50} = 18.2 ± 0.43 μM). Compound **4m** was the most active inhibitor (IC_{50} = 8.9 ± 0.31 μM), followed by **4e** (IC_{50} = 9.1 ± 0.21 μM), **4l** (IC_{50} = 10.7 ± 0.82 μM), **4c** (IC_{50} = 11.7 ± 0.36 μM), and **4f** (IC_{50} = 17.9 ± 0.56 μM). However, compounds **4d**, **4k**, **4n**, and **4p** depicted biological activity comparable to the standard acetazolamide with IC_{50} values in range of 18.3 ± 0.51–28.2 ± 0.01 μM, while compounds **4a**, **4b**, **4g**, **4h**, and **4j** were found

TABLE 2 | *In-vitro* inhibition results of compounds (**4a-p**) against *b*CA-II and *h*CA-II.

	Bovine carbonic anhydrase-II (*b*CA-II)		Human carbonic anhydrase-II (*h*CA-II)	
Compounds	**% Inhibition (0.5 mM)**	**IC_{50} ± SEM (μM)**	**% Inhibition (0.5 mM)**	**IC_{50} ± SEM (μM)**
4a	75.2	53.6 ± 0.85	75.2	59.6 ± 1.03
4b	83.6	67.3 ± 0.42	38.1	NA
4c	80.5	11.7 ± 0.36	88.5	21.1 ± 1.36
4d	92.9	19.7 ± 1.02	94.2	21.5 ± 0.52
4e	80.7	9.1 ± 0.21	92.7	39.9 ± 2.21
4f	88.9	17.9 ± 0.56	98.9	43.5 ± 1.51
4g	85.3	33.6 ± 0.22	85.3	14.0 ± 0.60
4h	92.4	38.0 ± 0.62	92.4	53.0 ± 2.12
4i	17.6	NA	27.8	NA
4j	78.6	46.6 ± 0.39	28.1	NA
4k	76.3	18.3 ± 0.51	36.2	NA
4l	78.2	10.7 ± 0.82	28.7	NA
4m	60.0	8.9 ± 0.31	30.5	NA
4n	54.2	28.2 ± 0.01	24.3	NA
4o	19.9	NA	89.4	22.0 ± 0.40
4p	87.3	26.8 ± 0.23	27.4	NA
Acetazolamide	86.4	18.2 ± 0.43	83.2	19.6 ± 1.23

SEM, Standard error mean; NA, Not active.

to be the least active hits of the series. For *h*CA-II, compounds **4a**, **4c**-**4h**, and **4o** were found to be active with IC_{50} values in the range of 14.0 ± 0.60–59.6 ± 1.03 μM, as compared to acetazolamide (IC_{50} = 19.6 ± 1.23 μM) (**Table 2**). Among all the compounds, **4g** (IC_{50} = 14.0 ± 0.60 μM) exhibited better activity than the standard drug, while compounds **4c** (IC_{50} = 21.1 ± 1.36 μM), **4d** (IC_{50} = 21.5 ± 0.52 μM), and **4o** (IC_{50} = 22.0 ± 0.40 μM) demonstrated activities comparable to acetazolamide. Compounds **4e** (IC_{50} = 39.9 ± 2.21 μM), **4f** (IC_{50} = 43.5 ± 1.51 μM), **4h** (IC_{50} = 53.0 ± 2.12 μM), and **4a** (IC_{50} = 59.6 ± 1.03 μM) were shown to be the least active hits in this series. The *in-vitro* results indicated that compounds **4g** and **4o** are more selective inhibitors for *h*CA-II. The biological activities of all the compounds are tabulated in **Table 2**.

Kinetics Studies

To investigate the mechanism of action of these compounds, kinetics studies were performed. The kinetics studies were used to discover the type of inhibition and dissociation constant (*Ki*). Kinetics studies of the most active compound, **4d**, against both *b*CA-II and *h*CA-II were performed, using different substrate concentrations on one side with different concentrations of **4d** on the other side. Compound **4d** inhibited both the *b*CA-II and *h*CA-II enzymes in a concentration-dependent manner with *Ki* values of 13.0 ± 0.013 and 14.25 ± 0.017 μM, respectively. From the kinetics studies, it was deduced that the compound **4d** is a competitive inhibitor for both *b*CA-II and *h*CA-II. The Lineweaver-Burk plots were used for determination of the type of inhibition, in which the reciprocal of substrate concentrations was plotted against the reciprocal of the rate of the reaction to monitor the effect of the inhibitor on both K_m and V_{max}. The Lineweaver-Burk plots of **4d** against both *b*CA-II and *h*CA-II clearly showed that the mode of inhibition of **4d** is competitive (**Figures 2A**, **3A**). In competitive inhibition, the K_m of enzyme increased, while V_{max} are not affected. The Lineweaver-Burk plots of compounds **4d** (**Figures 2A**, **3A**) showed that in the presence of compounds **4d**, the K_m of both enzymes *b*CA-II and *h*CA-II increased significantly on applying compounds **4d**, while the V_{max} remain unchanged, which described the competitive behavior of compounds **4d** and its interaction in the active site of the enzyme.

The K_i values of compounds **4d** for both enzymes *b*CA-II and *h*CA-II were deduced by secondary replots of Lineweaver-Burk plots by plotting the slope of each line in the Lineweaver-Burk

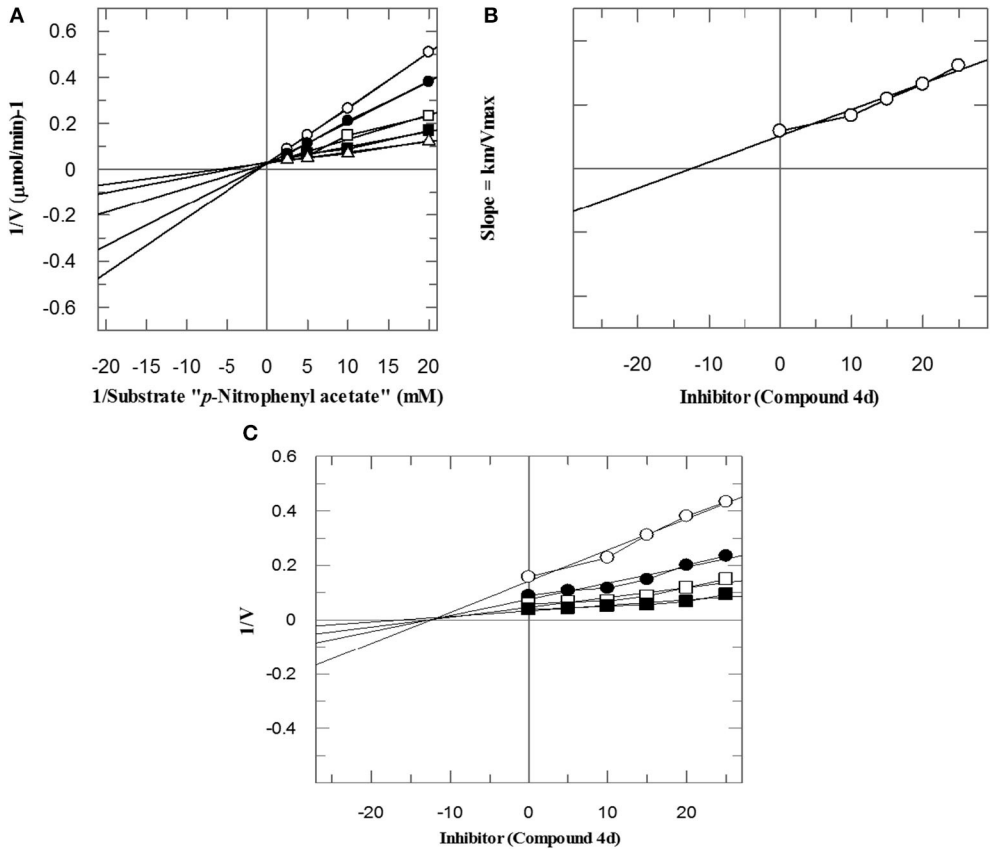

FIGURE 2 | The mode of inhibition of bCA-II by compound **4d**. **(A)** Lineweaver–Burk plot of reciprocal rate of reaction (velocities) vs. reciprocal of substrate (*p*-nitrophenyl acetate) in the absence (Δ), and in the presence of 14 μM (■), 17 μM (□), 20 μM (•), and 23 μM (○) of compound **4d**. **(B)** Secondary re-plot of Lineweaver–Burk plot between the slopes of each line on Lineweaver–Burk plot vs. different concentrations of compound **4d**. **(C)** Dixon plot of reciprocal rate of reaction (velocities) vs. different concentrations of compound **4d**.

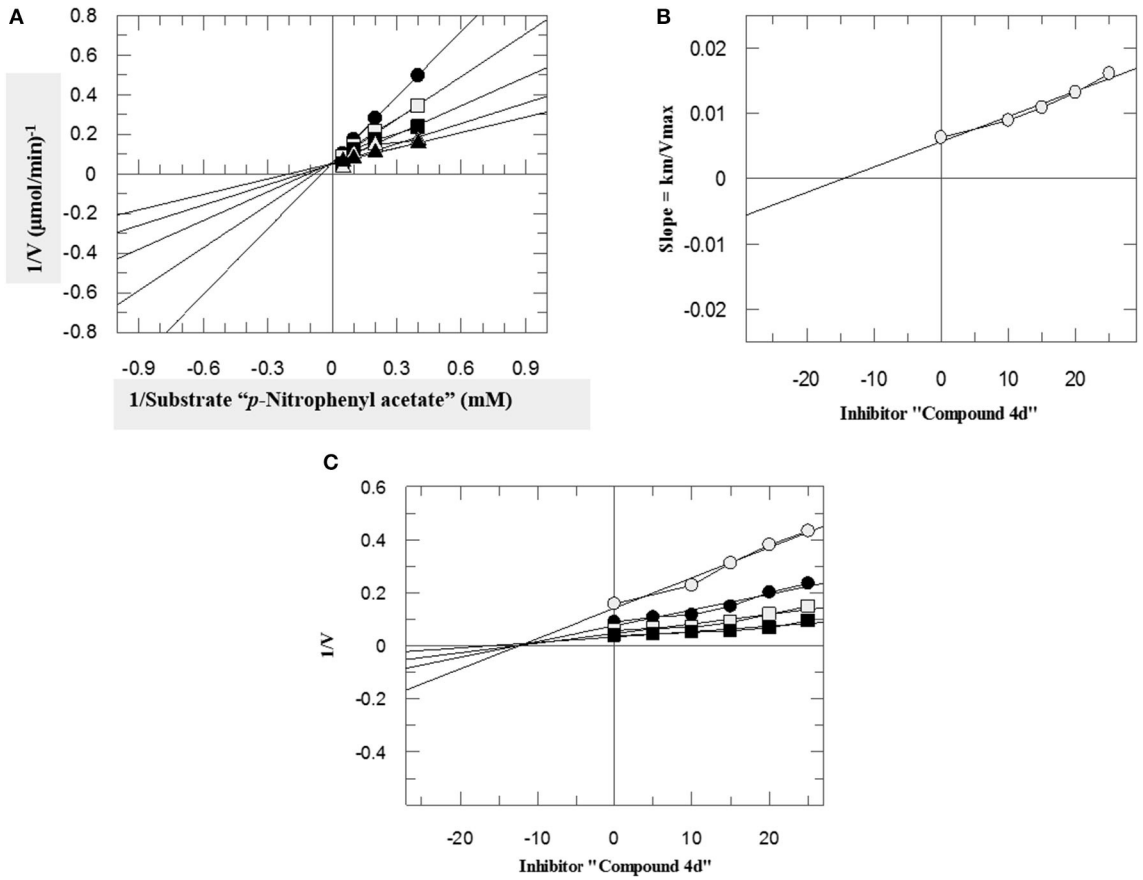

FIGURE 3 | The mode of inhibition of *h*CA-II by compound **4d**. **(A)** Lineweaver–Burk plot of reciprocal rate of reaction (velocities) vs. reciprocal of substrate (p-nitrophenyl acetate) in the absence (▲), and in the presence of 10 μM (Δ), 15 μM (■), 20 μM (□), and 25 μM (•) of compound **4d**. **(B)** Secondary re-plot of Lineweaver–Burk plot between the slopes of each line on Lineweaver–Burk plot vs. different concentrations of compound **4d**. **(C)** Dixon plot of reciprocal rate of reaction (velocities) vs. different concentrations of compound **4d**.

plots against different concentrations of compound **4d** (**Figures 2B**, **3B**). The K_i values were confirmed by Dixon plot after plotting the reciprocal of the rate of reaction against different concentrations of compound **4d** (**Figures 2C**, **3C**).

Computational Studies

Computational medicinal chemistry has expedited the pace of drug design and discovery over the last four decades (Lin et al., 2020). Docking is a computational method which is widely used to study and understand the interaction between two macro-molecules (for e.g., protein-protein or protein-DNA) or between a macromolecule and ligand (e.g., for a drug-receptor, drug-DNA, or drug-RNA) and effectively predict the inhibitory mechanism of drugs. Therefore, we predicted the mode of interactions of all the active compounds though molecular docking. The reference inhibitor (acetazolamide) and quinazolinones were docked into the catalytic active pocket of *h*CA-II and *b*CA-II. The binding modes and receptor-ligand interactions in the binding site of *b*CA-II and *h*CA-II in the three-dimensional and two-dimensional form were carefully examined by visual analysis through MOE. The results are presented in **Tables 3**, **4**. Molecular docking revealed that all the active quinazolinones derivatives were exactly fitted into the active catalytic pocket of both enzymes (*h*CA-II and *b*CA-II). The docked orientation of compounds revealed direct interactions of ligands with the zinc ion present in the active site. Moreover, interaction of compounds with the active site residues and water molecule stabilize the compounds in the active site.

The docking process was first validated by re-docking the standard inhibitor acetazolamide in the active site of enzyme and is presented in **Figures 4D**, **6D**.

Binding Interactions of Active Compounds and Their Predictive SAR Against *b*CA-II

From the docked poses of the all active compounds, it was confirmed that the compounds directly interact with Zn^{2+} ion through their quinazolinone-carbonyl moiety. Compounds **4c**, **4d**, **4e**, **4f**, **4k**, **4l**, and **4m** were found to be potent inhibitors of *b*CA-II with IC_{50} values in the range of 8.9–19.7 μM. Compound **4m** was the most potent inhibitor (IC_{50} = 8.9 ± 0.31μM), followed by **4e** > **4l** > **4c** > **4f** > **4k** > **4d**, while compounds **4p** > **4n** displayed moderate active, and **4g** > **4h** > **4j** >

TABLE 3 | Docking results of all active compounds against *b*CA-II.

Compounds	Docking score	Ligand atoms	Receptor atoms	Interaction type	Distance (Å)
4m	−5.50	O19	ZN	Metallic	3.48
		N18	OG1-THR198	HBD	3.19
		N9	NE2-GLN91	HBA	1.38
4e	−5.29		ZN	Metallic	3.58
		O19	HOH310	HBA	2.80
		N7	OG1-THR198	HBA	3.09
		N18	NE1-GLN91	HBA	3.17
		N9			
4l	−5.69	O19	ZN	Metallic	3.47
		N7	HG1-THR198	HBA	1.98
		N9	NE2-GLN91	HBA	3.06
4c	−6.14	O19	ZN	Metallic	3.16
		N20	ND2-ASN66	HBA	2.77
		N7	OG1-THR198	HBA	2.96
		O22	NE1-GLN92	HBA	3.02
4f	−5.70	O19	ZN	Metallic	3.51
		N7	HOH493	HBA	2.93
		N18	HOH279	HBA	1.27
4k	−5.36	O19	ZN	Metallic	3.44
		N7	OG1-THR198	HBA	1.96
		N9	OE2-GLN91	HBA	3.07
4d	−5.60	O19	ZN	Metallic	3.48
		N7	OG1-THR199	HBA	1.38
4p	−5.86	O19	ZN	Metallic	3.43
		N9	NE2-GLN91	HBD	3.38
		N18	OG1-THR198	HBA	2.55
4n	−5.27	O19	ZN	Metallic	3.54
		N18	OG1-THR198	HBD	1.77
		N9	NE2-GLN91	HBA	3.17
4g	−5.17	O11	OG1-THR198	HBA	2.81
		6-ring	ND2-ASN66	Pi-H	3.50
4h	−5.25	N19	OG1-THR198	HBA	2.99
4j	−5.72	N19	HOH-340	HBD	2.92
		O11	N-THR197	HBA	2.85
4a	−5.38	O11	OG1-THR198	HBA	2.07
4b	−4.99	N22	NE1-GLN91	HBD	3.11
		O11	HOH-435	HBA	2.65
Standard (Acetazolamide)	−5.17	N5	ZN	Metallic	3.35
		O10	NE1-GLN91	HBA	3.47
		N6	HOH463	HBD	1.33

HBA, Hydrogen bond acceptor; HBD, Hydrogen bond donor.

4a > **4b** were retrieved as the least active, as compared to standard acetazolamide. The docked pose of **4m** indicates that the quinazolinone-carbonyl moiety of **4m** formed a metallic bond (3.44 Å) with the Zn^{2+} ion, while the quinazolinone-nitrogen formed hydrogen bonds with the side chain of Thr198 and Gln91 at a distance of 2.28 and 3.41 Å, respectively. Similarly, carbonyl oxygen and the nitro groups of **4e** mediated a metallic bond with Zn^{2+} ion (3.58 Å), and H-bonds with the side chains of Thr198 (2.80 Å) and Gln91 (3.09 Å). Additionally, the quinazolinone substituted amino group of **4e** mediated a H-bond with a water molecule in the active site (3.17 Å). The third most active compounds, **4l** and **4c**, also followed a similar type of interaction, however, **4c** was also stabilized by the side chains of Asn66 and Gln92 through hydrogen bonding. The carbonyl oxygen of **4f** and **4k** interacted with the Zn^{2+} ion, however **4f** lost the interactions with Thr198 and Gln91, instead mediating H-bonding with two water molecules (WAT493 and WAT279), however **4k** retained H-bonds with Thr198 and Gln91. Compound **4d** showed a metallic and a H-bond with the Zn^{2+} ion and Thr199, respectively, however it lost the interactions with Gln91 and water molecules.

The quinazolinone moiety of the moderate active compounds (**4p** and **4n**) interacted with the Zn^{2+} ion, while the quinazolinone moiety of both the compounds mediated hydrogen bonding with the side chains of Gln91 and Thr198.

TABLE 4 | Computational analysis of all active compounds against *h*CA-II.

Code	Docking score	Ligand atoms	receptor Atoms	interaction type	Distance (Å)
4g	−4.51	N18	HOH270	HBD	2.45
		N18	ND2-ASN62	HBA	3.34
		N18	OG1-THR200	HBA	2.99
4c	−4.96	O20	NE2-GLN92	HBA	3.42
		N18	HOH270	HBA	2.78
4d	−5.36	O21	ZN	Metallic	2.73
		N11	OG1-THR200	HBA	2.68
4o	−5.31	O20	ZN	Metallic	2.71
		N7	NE2-GLN92	HBA	2.79
		N18	OG1-THR200	HBD	3.38
4e	−5.20	O20	ZN	Metallic	2.54
		N7	NE2-GLN92	HBA	2.65
4f	−4.43	N18	OG1-THR200	HBD	3.10
		O19	HOH270	HBA	2.89
4h	−4.73	N18	OG1-THR200	HBA	3.33
		O19	HOH270	HBA	2.38
4a	−4.44	O19	ND2-ASN62	HBD	1.89
		N18	OD1-ASN67	HBA	2.74
Standard (Acetazolamide)	−4.85	O10	ZN	Metallic	2.73
		O11	OG1-THR199	HBA	3.12
		O11	OG1-THR-200	HBD	3.60

HBA, Hydrogen bond acceptor; HBD, Hydrogen bond donor.

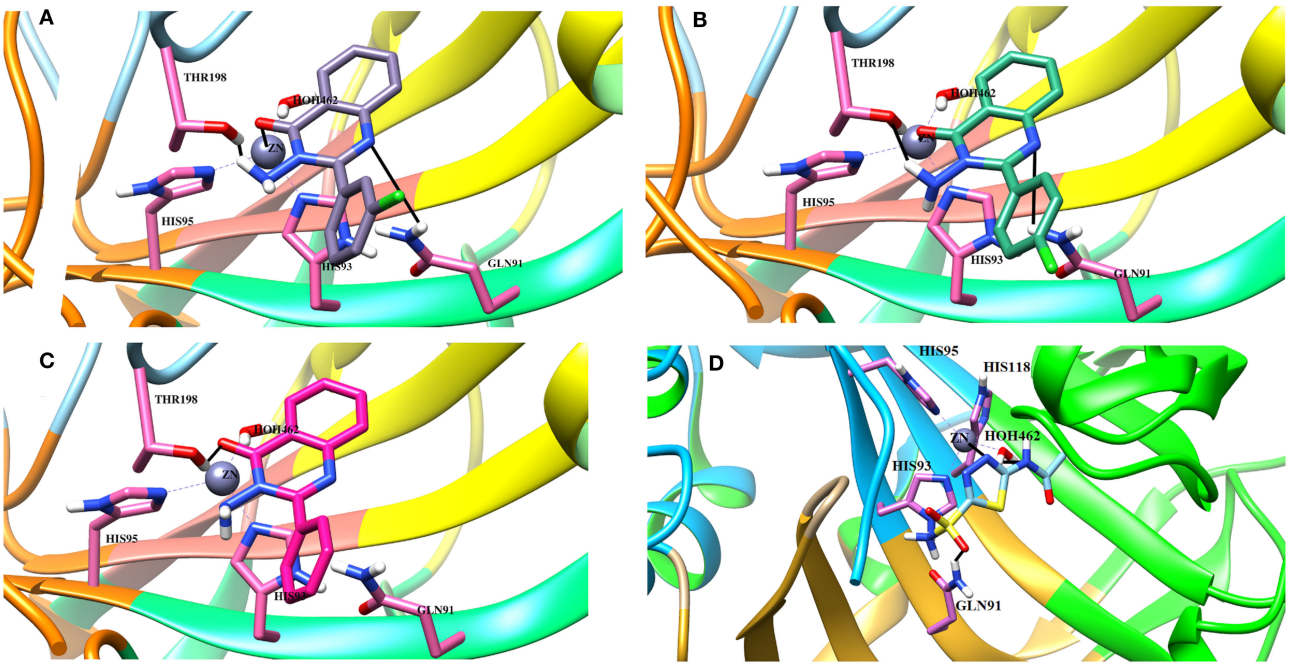

FIGURE 4 | The 3D interaction of the **(A)** most active compound (**4 m,** shown in gray stick model), **(B)** moderate active compound (**4n,** green stick model), **(C)** least active compound (**4a,** pink stick model), and **(D)** standard drug (acetazolamide, shown in cyan sticks) in the active site of bCA-II. The active site residues are depicted in pink stick model. The hydrogen bonds are presented in black lines.

The docked view of the least active compounds (**4g**, **4h**, **4j**, **4a**, and **4b**) showed that quinazolinone carbonyl of **4g** interacted with the side chain of Thr198 via H-bond (2.81 Å) and the side chain of Asn66 offered a hydrophobic interaction to the compound (3.50 Å). Whereas, quinazolinone-amide group of **4h** mediated a H- bond with the side chain of Thr198

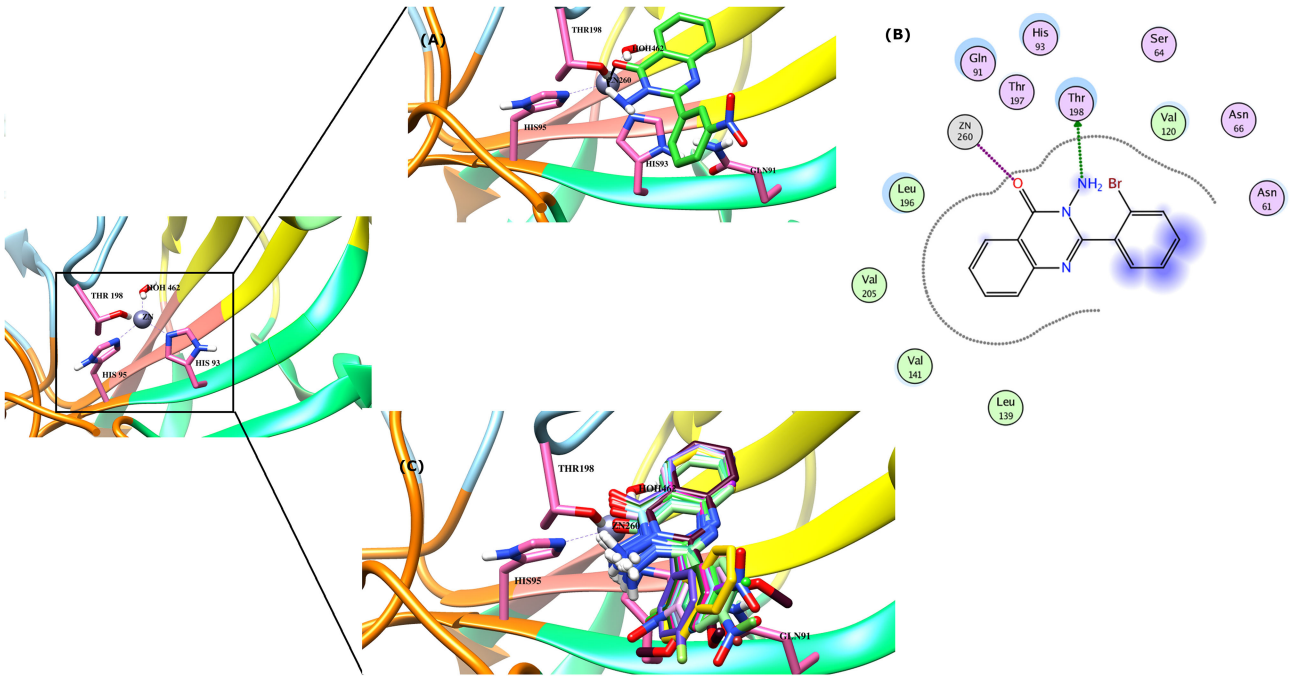

FIGURE 5 | (A) The docked view of compound **4d** is shown in the active site of *b*CA-II in 3D-form. **(B)** The binding interactions of **4d** in two-dimensional form is demonstrated. **(C)** The binding modes of all the active compounds are shown. The hydrogen bonds are shown in black lines.

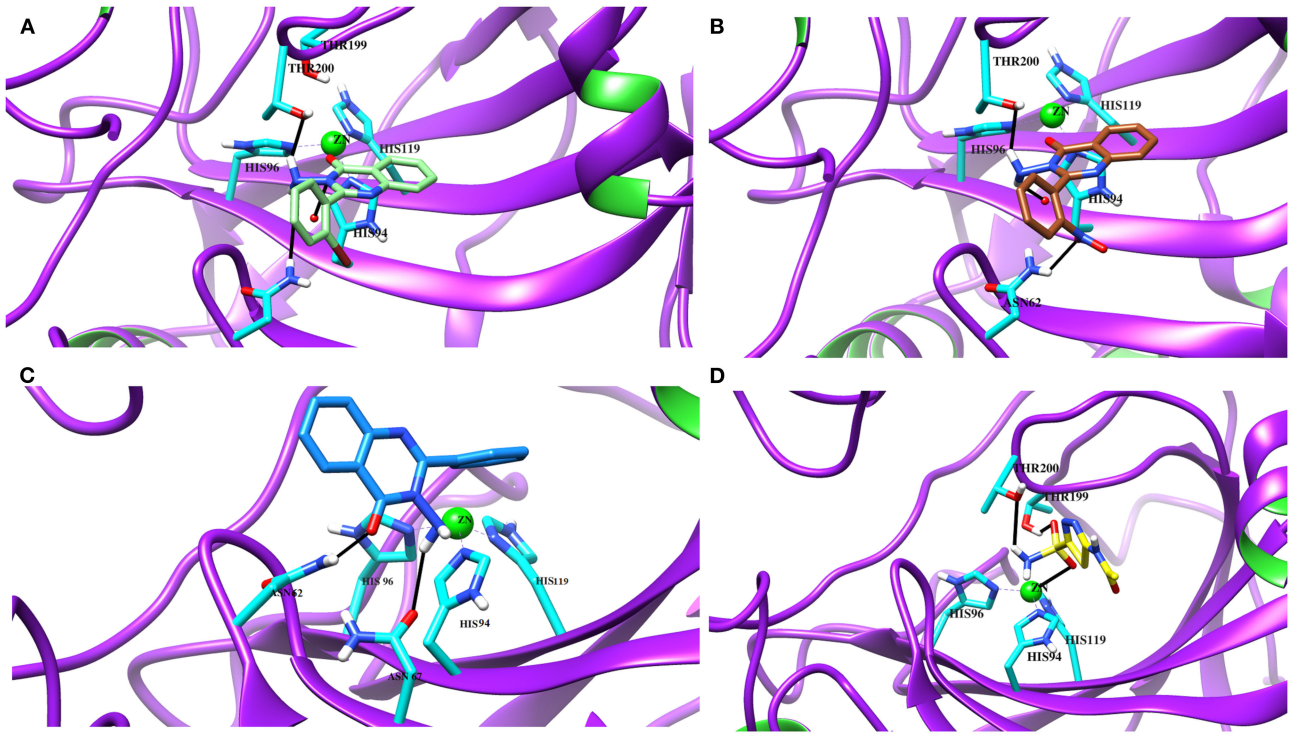

FIGURE 6 | The 3D docked view of the **(A)** most active compound (**4g**, showed as lime green stick model), **(B)** moderate active compound (**4c**, shown as green stick model) **(C)** least active compound (**4a**, shown as sky blue stick model) and **(D)** standard (acetazolamide shown as yellow stick model) against hCA-II. The active site residues are depicted in cyan stick model. The hydrogen bonds are presented in black lines.

(2.99 Å), and the amide group of **4j** interacted with a water molecule (WAT340) present in the active site. Similarly, the carbonyl oxygen and amide nitrogen of compounds **4a** and **4b** mediated H-bonds with the side chain of Thr197 and Gln91, respectively. Additionally, **4b** formed a bond with a water molecule (WAT435). The binding interactions and docking scores of each docked compound are tabulated in **Table 3**. **Figure 4** shows the binding interactions of the most active (**4m**), moderate (**4n**), and the least active (**4a**) compounds, however, a docked view of the most potent compound (**4d**) and all the compounds are presented in **Figure 5**.

Binding Interactions of Active Compounds and Their Predictive SAR Against *h*CA-II

Docking analysis deduced that the quinazolinone moieties of these compounds are responsible for the formation of metallic interactions with the Zn^{2+} atom in the catalytic cavity. Compound **4g** ($IC_{50} = 14.0 \pm 0.60\,\mu M$) was the most potent and selective inhibitor of *h*CA-II, as compared to standard acetazolamide ($IC_{50} = 19.6 \pm 1.23\,\mu M$), followed by compounds **4c** > **4d** > **4o** and least active **4e** > **4f** > **4h** > **4a**. The quinazolinone moiety of **4g** interacted with the side chain of Asn62, Thr200, and Wat270 with bond lengths of 3.34, 2.99, and 2.45 Å?, respectively. Similarly, **4c** interacted with the side chain of Gln92 and Wat270, whereas **4d** was linked with Zn^{2+} atom through its nitro-oxygen group. The nitro-oxygen and aminoquinoline moiety of **4o** interacted with Zn^{2+} atom and the side chains of Gln92 and Thr200 via hydrogen bonds. However, the quinazolinone moiety of **4e** interacted with the Zn^{2+} ion and Gln92. On the other hand, the least active compounds, **4a**, **4f**, and **4h**, interacted with the side chains of Asn62, Asn67, Thr200, and water molecules within the active site. The detailed binding interactions of active compounds and their docking scores are tabulated in **Table 4**. The binding interactions of most active (**4g**), moderate (**4c**), and least active (**4a**) compounds in the active site of *h*CA-II are presented in **Figure 6**. The docked orientation of all active compounds and the binding interaction of compound **4d** are shown in **Figure 7**.

CONCLUSION

Quinazolinone derivatives (**4a-p**) were synthesized in search of new therapeutic agents for glaucoma and other diseases associated with hyper activity of CA-II. The *in-vitro* results showed that these skeletons displayed moderate to significant inhibition of both the enzymes (*b*CA-II and *h*CA-II).

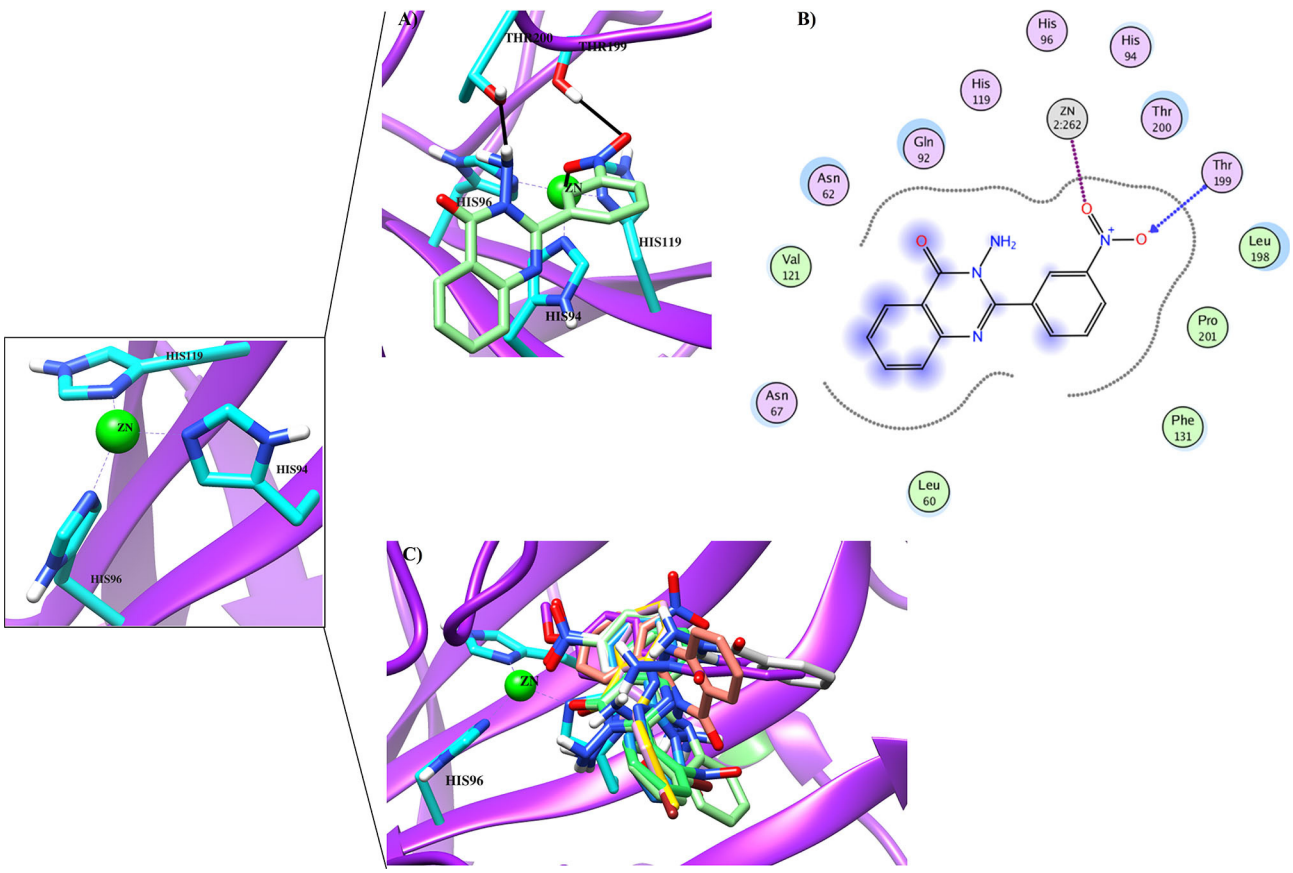

FIGURE 7 | (A) The docked view of compound **4d** (lime green stick mode) in the active site of *h*CA-II. **(B)** The 2D-binding interactions of 4**d** are presented **(C)** The docked orientation of all the active compound in the active site of *h*CA-II are shown.

Compounds **4c**, **4e**, **4f**, **4l**, and **4m** showed superior activity against *b*CA-II, while compounds **4g**, **4c**, **4d**, and **4o** were found to be significantly active against *h*CA-II. The structure-activity relationship reflected that the nitro group on phenyl ring at R position plays an important role in the overall inhibitory activities of compounds. Among the tested compounds, **4g** and **4o** are more selective for *h*CA-II. Moreover, kinetics studies showed the competitive behavior of inhibition of this series. Additionally, molecular docking predicted that the compounds bind efficiently with Zinc ion and several residues within the active site, therefore, through appropriate fitting and binding, these compounds effectively inhibit both *b*CA-II and *h*CA-II enzymes.

DATA AVAILABILITY STATEMENT

The original contributions presented in the study are included in the article/supplementary material, further inquiries can be directed to the corresponding author/s.

AUTHOR CONTRIBUTIONS

AA-H and ZS conceived and designed the study. ZK synthesized all compounds. AK and MK performed *in-vitro* assay. MK and SH performed the computational studies and analyzed the data. AK wrote the manuscript with input and comments from MK, SH, ZK, ZS, and AA-H. All authors have read and approved the final version of the manuscript.

FUNDING

The generous support of this project through project number (BFP/RGP/HSS/19/198).

ACKNOWLEDGMENTS

The authors would like to thank the University of Nizwa for the generous support of this project. We thank technical staff for assistance.

REFERENCES

(MOEv2014.09) *Molecular Operating Environment, Chemical Computing Group ULC*. Montreal, QC.

Achal, V., and Pan, X. (2011). Characterization of urease and carbonic anhydrase producing bacteria and their role in calcite precipitation. *Curr. Microbiol*. 62, 894–902. doi: 10.1007/s00284-010-9801-4

Aggarwal, M., Boone, C. D., Kondeti, B., and McKenna, R. (2013). Structural annotation of human carbonic anhydrases. *J. Enzyme Inhib. Med. Chem*. 28, 267–277. doi: 10.3109/14756366.2012.737323

Alaa, A.-M., Abou-Zeid, L. A., ElTahir, K. E. H., Mohamed, M. A., El-Enin, M. A. A., and El-Azab, A. S. (2016). Design, synthesis of 2, 3-disubstitued 4 (3*H*)-quinazolinone derivatives as anti-inflammatory and analgesic agents: COX-1/2 inhibitory activities and molecular docking studies. *Bioorg. Med. Chem*. 24, 3818–3828. doi: 10.1016/j.bmc.2016.06.026

Alafeefy, A. M., Carta, F., Ceruso, M., Al-Tamimi, A.-M. S., Al-Kahtani, A. A., and Supuran, C. T. (2016). Development of 3-(4-aminosulphonyl)-phenyl-2-mercapto-3H-quinazolin-4-ones as inhibitors of carbonic anhydrase isoforms involved in tumorigenesis and glaucoma. *Bioorg. Med. Chem*. 24, 1402–1407. doi: 10.1016/j.bmc.2016.02.011

Alafeefy, A. M., Ceruso, M., Al-Tamimi, A.-M. S., Del Prete, S., Capasso, C., and Supuran, C. T. (2014). Quinazoline–sulfonamides with potent inhibitory activity against the α-carbonic anhydrase from *Vibrio cholerae*. *Bioorg. Med. Chem*. 22, 5133–5140. doi: 10.1016/j.bmc.2014.08.015

Al-Amiery, A. A., Kadhum, A. A. H., Shamel, M., Satar, M., Khalid, Y., and Mohamad, A. B. (2014). Antioxidant and antimicrobial activities of novel quinazolinones. *Med. Chem. Res*. 23, 236–242. doi: 10.1007/s00044-013-0625-1

Al-Suwaidan, I. A., Alanazi, A. M., Alaa, A.-M., Mohamed, M. A., and El-Azab, A. S. (2013). Design, synthesis and biological evaluation of 2-mercapto-3-phenethylquinazoline bearing anilide fragments as potential antitumor agents: molecular docking study. *Bioorg. Med. Chem. Lett*. 23, 3935–3941. doi: 10.1016/j.bmcl.2013.04.056

Arslan, O. (2001). Inhibition of bovine carbonic anhydrase by new sulfonamide compounds. *Biochemistry* 66, 982–983. doi: 10.1023/A:1012365424900

Babu, Y. R., Bhagavanraju, M., Reddy, G. D., Peters, G. J., and Prasad, V. V. R. (2014). Design and synthesis of quinazolinone tagged acridones as cytotoxic agents and their effects on EGFR tyrosine kinase. *Arch. Pharm*. 347, 624–634. doi: 10.1002/ardp.201400065

Bari, A., Khan, Z. A., Shahzad, S. A., Naqvi, S. A. R., Khan, S. A., Amjad, H., et al. (2020). Design and syntheses of 7-nitro-2-aryl-4*H*-benzo [*d*][1, 3] oxazin-4-ones as potent anticancer and antioxidant agents. *J. Mol. Struct*. 1214:128252. doi: 10.1016/j.molstruc.2020.128252

Boriack-Sjodin, P. A., Zeitlin, S., Christianson, D. W., Chen, H. H., Crenshaw, L., Gross, S., et al. (1998). Structural analysis of inhibitor binding to human carbonic anhydrase II. *Protein Sci*. 7, 2483–2489. doi: 10.1002/pro.5560071201

Castillo, M. V., Romano, E., Raschi, A. B., Yurquina, A., and Brandán, S. A. (2012). Structural study and vibrational spectra of 3-amino-2-(4-chlorophenyl) quinazolin-4 (3*H*)-one. *Comput. Theor. Chem*. 995, 43–48. doi: 10.1016/j.comptc.2012.06.029

Chegwidden, W. R., Dodgson, S. J., and Spencer, I. M. (2000). "The roles of carbonic anhydrase in metabolism, cell growth and cancer in animals," in *The Carbonic Anhydrases, Vol*. 90, eds. W. R. Chegwidden, N. D. Carter, and Y. H. Edwards (Basel: Birkhäuser). doi: 10.1007/978-3-0348-8446-4_16

Edelsbrunner, H. (1992). *Weighted Alpha Shapes*. University of Illinois at Urbana-Champaign (Champaign, IL).

El-Azab, A. S., Alaa, A.-M., Bua, S., Nocentini, A., El-Gendy, M. A., Mohamed, M. A., et al. (2019). Synthesis of benzensulfonamides linked to quinazoline scaffolds as novel carbonic anhydrase inhibitors. *Bioorg. Chem*. 87, 78–90. doi: 10.1016/j.bioorg.2019.03.007

Frazier, M. L., Lilly, B. J., Wu, E. F., Ota, T., and Hewett-Emmett, D. (1990). Carbonic anhydrase II gene expression in cell lines from human pancreatic adenocarcinoma. *Pancreas* 5, 507–514. doi: 10.1097/00006676-199009000-00002

Gawad, N. M. A., Georgey, H. H., Youssef, R. M., and El Sayed, N. A. (2011). Design, synthesis, and anticonvulsant activity of novel quinazolinone analogues. *Med. Chem. Res*. 20, 1280–1286. doi: 10.1007/s00044-010-9465-4

He, D., Wang, M., Zhao, S., Shu, Y., Zeng, H., Xiao, C., et al. (2017). Pharmaceutical prospects of naturally occurring quinazolinone and its derivatives. *Fitoterapia* 119, 136–149. doi: 10.1016/j.fitote.2017.05.001

Hewett-Emmett, D. (2000). "Evolution and distribution of the carbonic anhydrase gene families," in *The Carbonic Anhydrases,* Vol. 90, eds W. R. Chegwidden, N. D. Carter, and Y. H. Edwards (Basel: Birkh?user). doi: 10.1007/978-3-0348-8446-4_3

Jakubowski, M., Szahidewicz-Krupska, E., and Doroszko, A. (2018). The human carbonic anhydrase II in platelets: an underestimated field of its activity. *Biomed Res. Int*. 2018:4548353. doi: 10.1155/2018/4548353

Khan, I., Ibrar, A., Abbas, N., and Saeed, A. (2014). Recent advances in the structural library of functionalized quinazoline and quinazolinone scaffolds: synthetic approaches and multifarious applications. *Eur. J. Med. Chem*. 76, 193–244. doi: 10.1016/j.ejmech.2014.02.005

Khan, I., Ibrar, A., Ahmed, W., and Saeed, A. (2015). Synthetic approaches, functionalization and therapeutic potential of quinazoline and quinazolinone skeletons: the advances continue. *Eur. J. Med. Chem*. 90, 124–169. doi: 10.1016/j.ejmech.2014.10.084

Khan, I., Zaib, S., Batool, S., Abbas, N., Ashraf, Z., Iqbal, J., et al. (2016). Quinazolines and quinazolinones as ubiquitous structural fragments in medicinal chemistry: an update on the development of synthetic methods and pharmacological diversification. *Biorg. Med. Chem*. 24, 2361–2381. doi: 10.1016/j.bmc.2016.03.031

Krishnamurthy, V. M., Kaufman, G. K., Urbach, A. R., Gitlin, I., Gudiksen, K. L., Weibel, D. B., et al. (2008). Carbonic anhydrase as a model for biophysical and physical-organic studies of proteins and protein– ligand binding. *Chem. Rev*. 108, 946–1051. doi: 10.1021/cr050262p

Lin, X., Li, X., and Lin, X. (2020). A review on applications of computational methods in drug screening and design. *Molecules* 25:1375. doi: 10.3390/molecules25061375

Lindskog, S. (1997). Structure and mechanism of carbonic anhydrase. *Pharmacol. Ther*. 74, 1–20. doi: 10.1016/S0163-7258(96)00198-2

Naïm, M., Bhat, S., Rankin, K. N., Dennis, S., Chowdhury, S. F., Siddiqi, I., et al. (2007). Solvated interaction energy (SIE) for scoring protein– ligand binding affinities. 1. exploring the parameter space. *J. Chem. Inf. Model* 47, 122–133. doi: 10.1021/ci600406v

Ozensoy Guler, O., Capasso, C., and Supuran, C. T. (2016). A magnificent enzyme superfamily: Carbonic anhydrases, their purification and characterization. *J. Enzyme Inhib. Med. Chem*. 31, 689–694. doi: 10.3109/14756366.2015.1059333

Pandit, U., and Dodiya, A. (2013). Synthesis and antitubercular activity of novel pyrazole–quinazolinone hybrid analogs. *Med. Chem. Res*. 22, 3364–3371. doi: 10.1007/s00044-012-0351-0

Panicker, C. Y., Varghese, H. T., Ambujakshan, K., Mathew, S., Ganguli, S., Nanda, A. K., et al. (2010). Vibrational spectra and computational study of 3-amino-2-phenyl quinazolin-4 (3H)-one. *J. Mol. Struct*. 963, 137–144. doi: 10.1016/j.molstruc.2009.10.026

Parkkila, A. K., Herva, R., Parkkila, S., and Rajaniemi, H. (1995). Immunohistochemical demonstration of human carbonic anhydrase isoenzyme II in brain tumours. *Histochem. J*. 27, 974–982. doi: 10.1007/BF02389687

Parkkila, S., Rajaniemi, H., Parkkila, A.-K., Kivelä J., Waheed, A., Pastoreková S., et al. (2000). Carbonic anhydrase inhibitor suppresses invasion of renal cancer cells *in vitro*. *Proc. Natl. Acad. Sci. U.S.A*. 97, 2220–2224. doi: 10.1073/pnas.040554897

Pastorekova, S., Parkkila, S., Parkkila, A. K., Opavsky, R., Zelnik, V., Saarnio, J., et al. (1997). Carbonic anhydrase IX, MN/CA IX: analysis of stomach complementary DNA sequence and expression in human and rat alimentary tracts. *Gastroenterology* 112, 398–408. doi: 10.1053/gast.1997.v112.pm9024293

Pastorekova, S., and Supuran, C. T. (2014). "Carbonic anhydrase IX: from biology to therapy," in *Hypoxia and Cancer* (Springer), 21–153. doi: 10.1007/978-1-4614-9167-5_6

Pocker, Y., and Meany, J. (1967). The catalytic versatility of erythrocyte carbonic anhydrase. II. Kinetic studies of the enzyme-catalyzed hydration of pyridine aldehydes. *Biochemistry* 6, 239–246. doi: 10.1021/bi00853a037

Ruusuvuori, E., and Kaila, K. (2014). "Carbonic anhydrases and brain pH in the control of neuronal excitability," in *Carbonic Anhydrase: Mechanism, Regulation, Links to Disease, and Industrial Applications: Subcellular Biochemistry*, Vol. 75 (Dordrecht: Springer). doi: 10.1007/978-94-007-7359-2_14

Saito, R., Sato, T., Ikai, A., and Tanaka, N. (2004). Structure of bovine carbonic anhydrase II at 1.95 Å resolution. *Acta Crystallogr. Sect. D Biol. Crystallogr*. 60, 792–795. doi: 10.1107/S0907444904003166

Sentürk, M., Gülçin, I., Beydemir, S., Küfrevioglu, Ö. I., and Supuran, C. T. (2011). *In vitro* inhibition of human carbonic anhydrase I and II isozymes with natural phenolic compounds. *Chem. Biol. Drug Des*. 77, 494–499. doi: 10.1111/j.1747-0285.2011.01104.x

Shaik, N. A., Bokhari, H. A., Masoodi, T. A., Shetty, P. J., Ajabnoor, G. M., Elango, R., et al. (2019). Molecular modelling and dynamics of CA2 missense mutations causative to carbonic anhydrase 2 deficiency syndrome. *J. Biomol. Struct. Dyn*. 38, 4067–4080. doi: 10.1080/07391102.2019.1671899

Shank, R. P., Doose, D. R., Streeter, A. J., and Bialer, M. (2005). Plasma and whole blood pharmacokinetics of topiramate: the role of carbonic anhydrase. *Epilepsy Res*. 63, 103–112. doi: 10.1016/j.eplepsyres.2005.01.001

Supuran, C. T. (2008). Carbonic anhydrases: novel therapeutic applications for inhibitors and activators. *Nat. Rev. Drug Discov*. 7, 168–181. doi: 10.1038/nrd2467

Supuran, C. T., and Scozzafava, A. (2007). Carbonic anhydrases as targets for medicinal chemistry. *Bioorg. Med. Chem*. 15, 4336–4350. doi: 10.1016/j.bmc.2007.04.020

Ur Rehman, N., Halim, S. A., Khan, M., Hussain, H., Yar Khan, H., Khan, A., et al. (2020). Antiproliferative and carbonic Anhydrase II inhibitory potential of chemical constituents from *Lycium shawi*i and *Aloe vera*: evidence from *in silico* target fishing and *in vitro* testing. *Pharmaceuticals* 13:94. doi: 10.3390/ph13050094

Zaraei, S.-O., El-Gamal, M. I., Shafique, Z., Amjad, S. T., Afridi, S., Zaib, S., et al. (2019). Sulfonate and sulfamate derivatives possessing benzofuran or benzothiophene nucleus as potent carbonic anhydrase II/IX/XII inhibitors. *Biorg Med Chem*. 27, 3889–3901. doi: 10.1016/j.bmc.2019.07.026

Conflict of Interest: The authors declare that the research was conducted in the absence of any commercial or financial relationships that could be construed as a potential conflict of interest.

The handling Editor declared a past co-authorship with one of the authors with the authors AK, SH, and AA-H.